The Astronomical Journal, 155:72 (9pp), 2018 February https://doi.org/10.3847/1538-3881/aaa292

A System of Three Super Earths Transiting the Late K-Dwarf GJ 9827 at 30 pc

Joseph E. Rodriguez[1], Andrew Vanderburg[1,2,6], Jason D. Eastman[1], Andrew W. Mann[2,3,7], Ian J. M. Crossfield[4], David R. Ciardi[5], David W. Latham[1], and Samuel N. Quinn[1]
[1] Harvard-Smithsonian Center for Astrophysics, 60 Garden Street, Cambridge, MA 02138, USA
[2] Department of Astronomy, The University of Texas at Austin, Austin, TX 78712, USA
[3] Department of Astronomy, Columbia University, 550 West 120th Street, New York, NY 10027, USA
[4] Department of Physics, Massachusetts Institute of Technology, Cambridge, MA, USA
[5] NASA Exoplanet Science Institute, California Institute of Technology, Pasadena, CA, USA
Received 2017 September 6; revised 2017 December 13; accepted 2017 December 14; published 2018 January 19

Abstract

We report the discovery of three small transiting planets orbiting GJ 9827, a bright ($K = 7.2$) nearby late K-type dwarf star. GJ 9827 hosts a $1.62 \pm 0.11\,R_\oplus$ super Earth on a 1.2 day period, a $1.269^{+0.087}_{-0.089}\,R_\oplus$ super Earth on a 3.6 day period, and a $2.07 \pm 0.14\,R_\oplus$ super Earth on a 6.2 day period. The radii of the planets transiting GJ 9827 span the transition between predominantly rocky and gaseous planets, and GJ 9827 b and c fall in or close to the known gap in the radius distribution of small planets between these populations. At a distance of 30 pc, GJ 9827 is the closest exoplanet host discovered by *K2* to date, making these planets well-suited for atmospheric studies with the upcoming *James Webb Space Telescope*. The GJ 9827 system provides a valuable opportunity to characterize interior structure and atmospheric properties of coeval planets spanning the rocky to gaseous transition.

Key words: planetary systems – planets and satellites: detection – stars: individual (GJ 9827)

Supporting material: data behind figure

1. Introduction

With the confirmation of over 3500 planets to date and an additional ∼4500 candidates from *Kepler* (Thompson et al. 2017), the focus of studying exoplanets has largely shifted from pure discovery to understanding planetary demographics, system architectures, interior structures, and atmospheres. In particular, planets that transit their host stars are valuable for understanding the properties of small planets in detail. Like an eclipsing binary star, combining the transit light curve with radial velocity observations yields a measurement of the mass and radius of a planet relative to its star, which constrain the planet's interior structure. Planetary atmospheres can also be studied if the planet transits. The opacity of a planet's atmosphere depends on its chemical composition and the wavelength of the observation. This causes the apparent size of the planet to change as a function of wavelength. Therefore, by measuring the depth of the transit as a function of wavelength, it is possible to gain insight into the composition and temperature of the planet's atmosphere (this technique is known as transit transmission spectroscopy; Seager & Sasselov 2000; Brown 2001; Fortney et al. 2003).

Our ability to study the interior structures and atmospheres of planets, especially small planets ($<3\,R_\oplus$) with small radial velocity and atmospheric signals, is highly dependent on the brightness of its host star. The brighter the host star, the easier it is to attain high enough signal-to-noise ratios to search for the small signals produced by small planets. The relative size of the planet to its host star is also highly important for transit transmission spectroscopy. It is easier to detect the small, wavelength-dependent changes in transit depth when planets are larger compared to their host stars, so small stars are more favorable targets than large stars for transit spectroscopy measurements. Therefore, nearby bright small stars with planets are excellent targets for atmospheric characterization (Burrows 2014).

Multi-planet systems provide the opportunity to compare the atmospheres and interior structures of different planets while accounting for many confounding variables, like formation history and composition. In some cases, like the recently discovered seven-planet system transiting the nearby late M-dwarf TRAPPIST-1 (Gillon et al. 2016, 2017), it is possible to study similarly sized planets across orders of magnitude in incident flux. In terms of the stellar irradiation of the seven planets, TRAPPIST-1 c resembles Venus, TRAPPIST-1 d resembles the Earth, and TRAPPIST-1 f is similar to Mars (Gillon et al. 2017).

However, it would also be desirable to find a multi-planet system suitable for characterization that has planets with different sizes in order to understand the compositions of small planets ranging in size from similar to Earth to about four times the size of Earth. The *Kepler* mission has found a nearly ubiquitous population of planets with radii larger than the Earth but smaller than Neptune (Howard et al. 2012; Batalha et al. 2013; Petigura et al. 2013; Morton & Swift 2014; Christiansen et al. 2015; Dressing & Charbonneau 2015) for which we have no analogue in our own solar system. Recently, the California *Kepler* Survey measured precise radii for over 2000 *Kepler* planets and found a bimodal distribution in the radii of small planets, with a deficit of planets with radii between 1.5 and $2.0\,R_\oplus$ and two peaks in the radius distribution at about $1.3\,R_\oplus$ and $2.5\,R_\oplus$ (Fulton et al. 2017). The deficit in radii around $1.5–2\,R_\oplus$ is coincident with the transition (Weiss & Marcy 2014; Rogers 2015) between predominantly rocky planets (typically smaller than $1.6\,R_\oplus$) and planets with substantial gaseous envelopes (typically larger than $1.6\,R_\oplus$) as determined from mass measurements of a large number of sub-Neptune-sized planets discovered by *Kepler* (Wu & Lithwick 2013; Hadden & Lithwick 2014, 2017; Marcy et al. 2014). As most of these planets with mass measurements orbit very close to

[6] NASA Sagan Fellow.
[7] NASA Hubble Fellow.

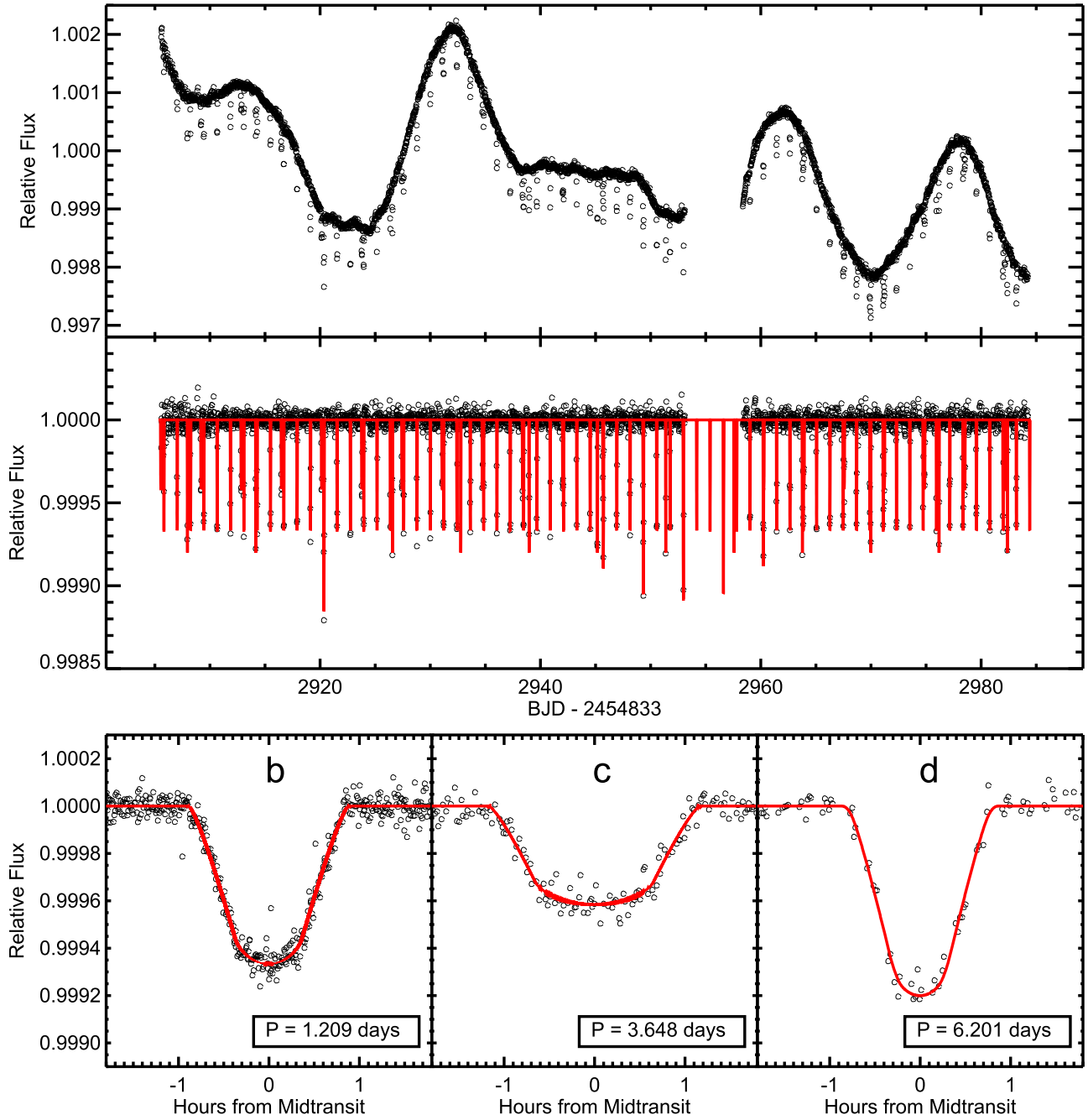

Figure 1. Top panel: the full K2 light curve of GJ 9827 from Campaign 12, corrected for systematics using the technique described in Vanderburg & Johnson (2014) and Vanderburg et al. (2016c). Middle panel: the corrected K2 light curve with best-fit low frequency variability removed. Bottom panel: phase-folded *K2* light curves of GJ 9827 b, c.#, and d. The observations are plotted in open black circles, and the best-fit models are plotted in red. The data used to create this figure are available.

their host stars ($P < 100$ days), they receive a large amount of high-energy irradiation that can evaporate gaseous envelopes made of H/He (Yelle 2004; Tian et al. 2005; Murray-Clay et al. 2009; Owen & Jackson 2012). The observed lack of planets with radii of 1.5–2.0 $R_\oplus$ could be due to these gaseous envelopes being evaporated away and leaving the smaller denser cores (Jin & Mordasini 2017; Owen & Wu 2017).

In this paper, we present the discovery of three transiting planets orbiting the nearby ($d = 30.3 \pm 1.6$ pc) star GJ 9827 using data from the *K2* mission. The planets transiting GJ 9827 are the closest planets discovered by K2 (surpassing K2-18, at 34 ± 4 pc Montet et al. 2015; Crossfield et al. 2016; Benneke et al. 2017). GJ 9827 b, c, and d are all super-Earth-sized with radii $R_b = 1.62 \pm 0.11\,R_\oplus$, $R_c = 1.269^{+0.087}_{-0.089}\,R_\oplus$, $R_d = 2.07 \pm 0.14\,R_\oplus$. Planets b ($P_b = 1.209$ days) and c ($P_c = 3.648$ days) orbit about half a percent outside of a 1:3 mean motion resonance, while planet d ($P_d = 6.201$) orbits far from integer period ratios with the other two planets. The host is a bright ($J \approx 8$, $H \approx 7.4$, $K \approx 7.2$) nearby late K star, making it an excellent target for atmospheric characterization with the upcoming *James Webb Space Telescope* (Gardner et al. 2006). The planets span the transition from rocky to gaseous planets, so the characteristics of their atmospheres and interior structures may illuminate how the structure and composition of small planets change with radius.

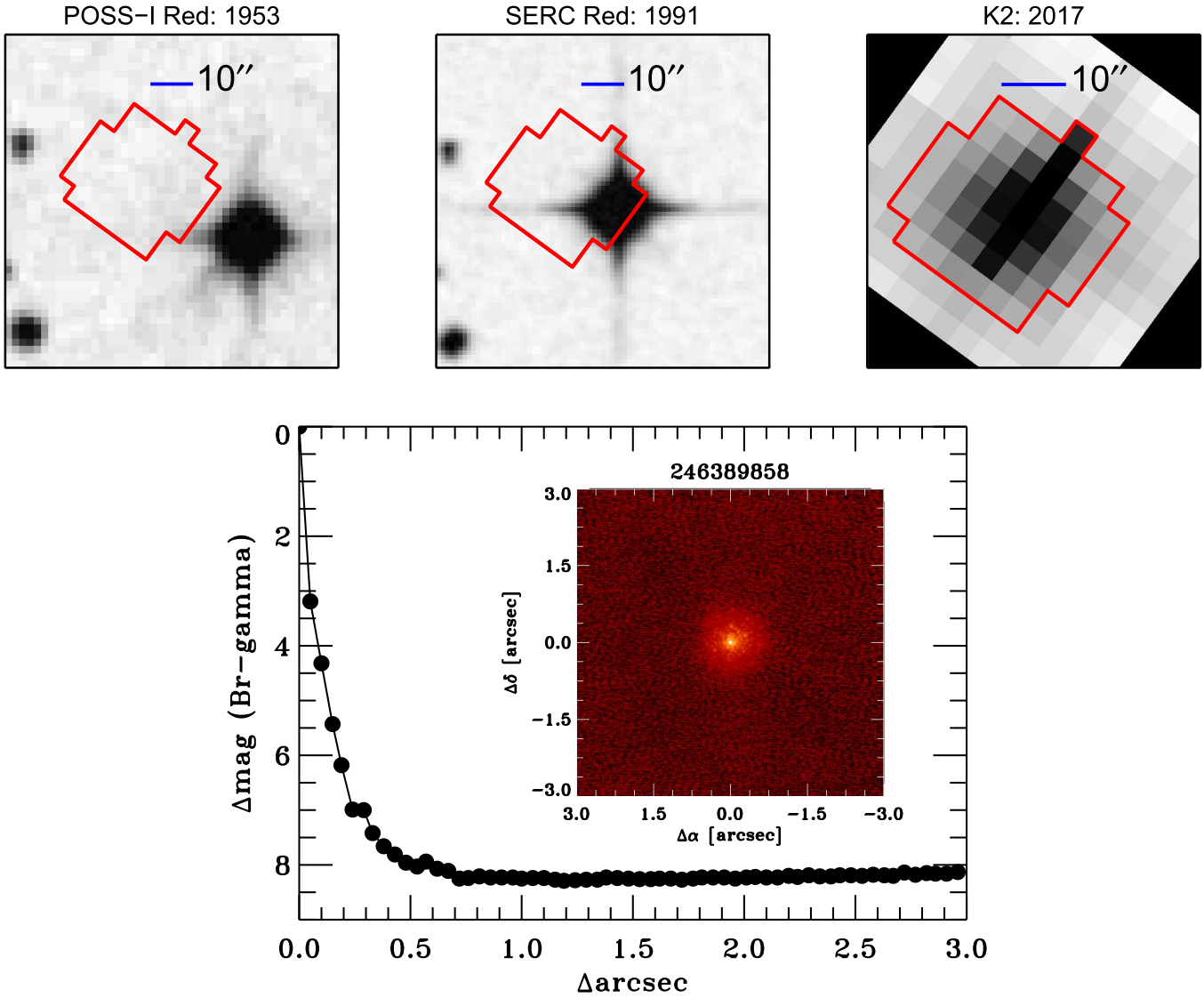

Figure 2. Top left panel: archival imaging from the National Geographic Society Palomar Observatory Sky Survey (NGS POSS) of GJ 9827 taken with a red emulsion in 1953. Top middle panel: archival imaging from the ESO/SERC survey of GJ 9827 taken with a red emulsion in 1991. Top right panel: summed image of GJ 9827 from K2 observations. The aperture selection is described in Vanderburg et al. (2016a). Bottom panel: the Keck Br-γ contrast curve and image (inset) of GJ 9827. We find no evidence of any additional components in the system.

2. Observations and Archival Data

2.1. K2 Photometry

In 2013 May, the *Kepler* spacecraft experienced a failure of the second of its four reaction wheels, ending its primary mission. However, the *Kepler* spacecraft has been re-purposed to obtain high precision photometry for ∼80 days at a time on a set of fields near the ecliptic in its extended *K2* mission (Howell et al. 2014). During K2 Campaign 12, GJ 9827 was observed from UT 2016 December 16 until UT 2017 March 04. We identified GJ 9827 as a candidate planet host after downloading all of the *Kepler*-pipeline calibrated target pixel files from the Mikulski Archive for Space Telescopes, producing light curves, and correcting for K2 spacecraft systematics following Vanderburg & Johnson (2014) and Vanderburg et al. (2016c). We then searched the resulting light curves for transiting planet candidates using the pipeline described by Vanderburg et al. (2016c). Among the objects uncovered in our search were three super-Earth-sized planet candidates with periods of 1.2, 3.6, and 6.2 days around the nearby star GJ 9827. After we identified the signals, we re-processed the K2 light curve to simultaneously fit the transits, stellar variability, and K2 systematics. We flattened the light curve by dividing away the best-fit stellar variability (which we modeled as a basis spline with breakpoints every 0.75 days) from our simultaneous fit to the light curve. The final light curve has a noise level of 39 ppm per 30 minute cadence exposure, and a 6 hr photometric precision of 9 ppm. See Figure 1 for the final light curve.

The K2 light curve shows rotational stellar variability on GJ 9827 with a typical amplitude of about 0.2% peak to peak (see Figure 1). We calculated the autocorrelation function of the K2 light curve and found a rotation period of 31 ± 1 days, although it is possible the true rotation period is at about 16 days, or half our best estimate. The autocorrelation function preferred a 31 day period most likely because of the flatness at $\mathrm{BJD_{TDB}}$-2454833 = 2945 instead of another peak.

Table 1
GJ 9827 Magnitudes and Kinematics

Other identifiers	HIP 115752 2MASS J23270480-0117108 EPIC 246389858		
Parameter	Description	Value	Source
α_{J2000}	Right Ascension (R.A.)	23:27:04.83647	1
δ_{J2000}	Declination (Decl.)	−01:17:10.5816	1
B_T	Tycho B_T mag	12.10 ± 0.178	2
V_T	Tycho V_T mag	10.648 ± 0.069	2
B	APASS Johnson B mag	11.569 ± 0.034	3
V	APASS Johnson V mag	10.250 ± 0.138	3
g'	APASS Sloan g' mag	10.995 ± 0.021	3
r'	APASS Sloan r' mag	9.845	3
i'	APASS Sloan i' mag	9.394	3
J	2MASS J mag	7.984 ± 0.02	4, 5
H	2MASS H mag	7.379 ± 0.04	4, 5
K_S	2MASS K_S mag	7.193 ± 0.020	4, 5
WISE1	*WISE1* mag	6.990 ± 0.041	6
WISE2	*WISE2* mag	7.155 ± 0.02	6
WISE3	*WISE3* mag	7.114 ± 0.017	6
WISE4	*WISE4* mag	6.957 ± 0.107	6
μ_α	NOMAD proper motion in RA (mas yr^{-1})	374.4 ± 2.2	7
μ_δ	NOMAD proper motion in DEC (mas yr^{-1})	215.7 ± 1.9	7
$v \sin i_\star$	Rotational velocity	1.3 ± 1.5 km s^{-1}	8
[m/H]	Metallicity	−0.5 ± 0.1	8
$T_{\rm eff}$	Effective Temperature	4270 ± 100 K	8
log(g)	Surface Gravity	4.9 ± 0.2 (cgs)	8
π	*Hipparcos* Parallax (mas)	32.98 ± 1.76	1
d	Distance (pc)	30.32 ± 1.62	1
Spec. Type	Spectral Type	K5V	9

References. (1) van Leeuwen (2007), (2) Høg et al. (2000) (3) Henden et al. (2015), (4) Cutri et al. (2003), (5) Skrutskie et al. (2006), (6) Cutri et al. (2014), (7) Zacharias et al. (2004), (8) Houdebine et al. (2016), (9) Reid et al. (1995).

2.2. Archival Spectroscopy

As part of a survey of nearby solar-type stars, GJ 9827 was observed on UT 2000 August 31 using the Center for Astrophysics Digital Speedometer on the 1.5 m Wyeth Reflector at the Oak Ridge Observatory in the town of Harvard, Massachusetts. The Digital Speedometer measured an absolute RV of 31.2 km s^{-1} with an approximate accuracy of ∼0.3 km s^{-1} (Latham, private communication). GJ 9827 was also observed on UT 2010 October 08 and UT 2011 August 06 using a CORAVEL-type spectrometer at Vilnius University Observatory, which measured absolute RVs of GJ 9827 on these dates of 32.6 km s^{-1} and 31.1 km s^{-1}, respectively (Sperauskas et al. 2016). Using the equations given in Johnson & Soderblom (1987), the *UVW* space velocities of GJ 9827 were estimated to be $(U,V,W) = (-59.2, 20.9, 30.6)$ km s^{-1} (Sperauskas et al. 2016). Using the probability distributions of Reddy et al. (2006), GJ 9827 is predicted to be a member of the Galactic thin disk. From these observations, we see no evidence of any large RV variation over the span of over 10 years.

GJ 9827 was also observed twice in 2004 with the High Accuracy Radial Velocity Planet Searcher (HARPS) spectrograph as part of the guaranteed time collaboration's planet search, but not enough observations were taken to identify the small planet candidates we find. Later, Houdebine et al. (2016) used a principal component analysis-based method to analyze the HARPS spectra and estimate stellar parameters. They found: $T_{\rm eff} = 4270 \pm 100$, $[{\rm Fe/H}] = -0.5 \pm 0.1$ dex, $\log g = 4.9 \pm 0.2$, and $v \sin i_\star = 1.3^{+1.5}_{-1.3}$ km s^{-1}. From the *Hipparcos* parallax and an analysis of the spectral energy distribution (SED), Houdebine et al. (2016) estimated the radius of GJ 9827 to be R_* of 0.623 ± 0.082 $R_\odot$. In this paper, we adopt the spectroscopic parameters from Houdebine et al. (2016) but derive our own stellar mass and radius for our global modeling (described in Section 3).

2.3. Archival Seeing-limited Imaging

Using archival observations from the National Geographic Society Palomar Observatory Sky Survey (NGS POSS) from 1953 and 1991 (ESO/SERC), we looked for nearby bright companions that may dilute our observed transit depths. GJ 9827 has a high proper motion ($\mu_\alpha = 374.4$ mas and $\mu_\delta = 215.7$ mas) and has moved nearly 30″ from its original position when the POSS image was taken in 1953 (See Figure 2). In 1953, GJ 9827 was outside of the region of sky enclosed within the photometric aperture we use to produce its modern K2 light curve. No background stars are present inside our K2 photometric aperture down to the POSS limiting magnitude of about $R = 20$, a full 10 mag fainter than GJ 9827. As all three transit signals around GJ 9827 have depths greater than 100 ppm, the maximum depth of a transit caused by a background star 10 mag fainter than GJ 9827, we can use "patient imaging" to confidently rule out background stars as the sources of these transit signals.

2.4. Keck/NIRC2 AO Imaging

Using the Near Infrared Camera 2 (NIRC2) behind the natural guide star adaptive optics system at the W. M. Keck Observatory, we obtained high-resolution images of GJ 9827 using the Br-γ filter on UT 2017 August 19. NIRC2 has a 1024 × 1024 pixel array with a 9.942 mas pix^{-1} pixel scale. The lower left quadrant of the NIRC2 array suffers from a higher noise level, and a three-point dither pattern was adopted excluding this regime of the detector. After flat-fielding and sky subtraction, each observation was shifted and co-added, resulting in the final image shown in Figure 2. No other star was detected in the 10″ field of view. To determine our sensitivity to companions, we inject simulated sources into the final image that have a signal to noise of 5. Figure 2 shows the 5σ sensitivity as a function of spatial separation from GJ 9827, and the inset shows the image itself.

3. System Modeling

Making use of the flattened *K2* light curves, the *Hipparcos* parallax, and stellar parameters, we perform a global fit of the GJ 9827 system using EXOFASTv2 (Eastman et al. 2013; Eastman 2017, J. D. Eastman et al. 2017, in preparation). EXOFASTv2 is based heavily on EXOFAST, but a large

Table 2
Median Values and 68% Confidence Interval for GJ 9827

Parameter	Units	Values		
Stellar Parameters				
M_*	Mass ($M_\odot$)	$0.614^{+0.030}_{-0.029}$		
R_*	Radius ($R_\odot$)	$0.613^{+0.033}_{-0.034}$		
ρ_*	Density (cgs)	$3.76^{+0.75}_{-0.57}$		
$\log g$	Surface gravity (cgs)	$4.651^{+0.055}_{-0.050}$		
T_{eff}	Effective Temperature (K)	4269^{+98}_{-99}		
Planetary Parameters:		b	c	d
a	Semimajor axis (au)	$0.01888^{+0.00030}_{-0.00031}$	$0.03942^{+0.00062}_{-0.00064}$	$0.05615^{+0.00089}_{-0.00091}$
P	Period (days)	$1.2089802^{+0.0000084}_{-0.0000081}$	$3.648083^{+0.000060}_{-0.000058}$	$6.201467^{+0.000062}_{-0.000061}$
M_P	Mass ($M_\oplus$)	$3.42^{+1.2}_{-0.76}$	$2.42^{+0.75}_{-0.49}$	$5.2^{+1.8}_{-1.2}$
R_P	Radius ($R_\oplus$)	1.62 ± 0.11	$1.269^{+0.087}_{-0.089}$	2.07 ± 0.14
i	Inclination (Degrees)	$85.73^{+1.2}_{-0.96}$	$88.05^{+0.64}_{-0.48}$	$87.39^{+0.20}_{-0.18}$
ρ_P	Density (cgs)	$4.50^{+1.5}_{-0.98}$	$6.4^{+2.0}_{-1.1}$	$3.23^{+1.1}_{-0.72}$
$\log g_P$	Surface gravity	$3.110^{+0.12}_{-0.098}$	$3.163^{+0.11}_{-0.082}$	$3.07^{+0.12}_{-0.10}$
$T_{\rm eq}$	Equilibrium temperature (K)	1172 ± 43	811 ± 30	680 ± 25
Θ	Safronov Number	$0.00460^{+0.0015}_{-0.00096}$	$0.0086^{+0.0025}_{-0.0016}$	$0.0162^{+0.0052}_{-0.0035}$
$\langle F \rangle$	Incident Flux (10^9 erg s^{-1}cm^{-2})	$0.429^{+0.066}_{-0.060}$	$0.098^{+0.015}_{-0.014}$	$0.0485^{+0.0074}_{-0.0068}$
T_C	Time of Transit ($\rm BJD_{TDB}$)	$2457738.82588^{+0.00030}_{-0.00031}$	$2457742.19944^{+0.00063}_{-0.00068}$	$2457740.96111 \pm 0.00044$
T_P	Time of Periastron ($\rm BJD_{TDB}$)	$2457738.82588^{+0.00030}_{-0.00031}$	$2457742.19944^{+0.00063}_{-0.00068}$	$2457740.96111 \pm 0.00044$
T_S	Time of Eclipse ($\rm BJD_{TDB}$)	$2457739.43037 \pm 0.00030$	$2457744.02348^{+0.00061}_{-0.00066}$	$2457744.06185 \pm 0.00041$
T_A	Time of Ascending Node ($\rm BJD_{TDB}$)	$2457738.52363^{+0.00030}_{-0.00031}$	$2457741.28742^{+0.00065}_{-0.00069}$	$2457739.41074 \pm 0.00045$
T_D	Time of Descending Node ($\rm BJD_{TDB}$)	$2457739.12812^{+0.00030}_{-0.00031}$	$2457743.11146^{+0.00062}_{-0.00067}$	$2457742.51148^{+0.00042}_{-0.00043}$
K	RV semi-amplitude (m s^{-1})	$2.84^{+0.97}_{-0.64}$	$1.39^{+0.44}_{-0.29}$	$2.50^{+0.86}_{-0.58}$
$\log K$	Log of RV semi-amplitude	$0.45^{+0.13}_{-0.11}$	$0.14^{+0.12}_{-0.10}$	$0.40^{+0.13}_{-0.12}$
$M_P \sin i$	Minimum mass ($M_\oplus$)	$3.41^{+1.2}_{-0.76}$	$2.42^{+0.75}_{-0.49}$	$5.2^{+1.8}_{-1.2}$
M_P/M_*	Mass ratio	$0.0000168^{+0.0000058}_{-0.0000038}$	$0.0000119^{+0.0000037}_{-0.0000025}$	$0.0000254^{+0.0000089}_{-0.0000060}$
R_P/R_*	Radius of planet in stellar radii	$0.02420^{+0.00040}_{-0.00047}$	$0.01899^{+0.00034}_{-0.00037}$	$0.03093^{+0.00065}_{-0.00059}$
a/R_*	Semimajor axis in stellar radii	$6.62^{+0.41}_{-0.35}$	$13.83^{+0.86}_{-0.74}$	$19.7^{+1.2}_{-1.0}$
d/R_*	Separation at mid transit	$6.62^{+0.41}_{-0.35}$	$13.83^{+0.86}_{-0.74}$	$19.7^{+1.2}_{-1.0}$
b	Impact parameter	$0.493^{+0.080}_{-0.12}$	$0.469^{+0.085}_{-0.13}$	$0.896^{+0.012}_{-0.016}$
δ	Transit depth	$0.000586^{+0.000019}_{-0.000023}$	$0.000361^{+0.000013}_{-0.000014}$	$0.000957^{+0.000041}_{-0.000036}$
Depth	Flux decrement at mid transit	$0.000586^{+0.000019}_{-0.000023}$	$0.000361^{+0.000013}_{-0.000014}$	$0.000957^{+0.000041}_{-0.000036}$
P_T	A priori non-grazing transit prob	$0.1474^{+0.0082}_{-0.0086}$	$0.0710^{+0.0040}_{-0.0042}$	$0.0492^{+0.0027}_{-0.0029}$
$P_{T,G}$	A priori transit prob	$0.1547^{+0.0088}_{-0.0092}$	$0.0737^{+0.0042}_{-0.0044}$	$0.0524^{+0.0030}_{-0.0031}$
$T_{\rm FWHM}$	FWHM duration (days)	$0.05083^{+0.00080}_{-0.00072}$	$0.0743^{+0.0011}_{-0.0012}$	$0.04398^{+0.0010}_{-0.00094}$
τ	Ingress/egress duration (days)	$0.00163^{+0.00023}_{-0.00022}$	$0.00181^{+0.00025}_{-0.00024}$	$0.00708^{+0.00098}_{-0.00094}$
T_{14}	Total duration (days)	$0.05249^{+0.00074}_{-0.00071}$	0.0761 ± 0.0011	$0.0511^{+0.0011}_{-0.0010}$
Wavelength Parameters:		*Kepler*		
$u_{1,Kepler}$	linear limb-darkening coeff	$0.417^{+0.069}_{-0.053}$		
$u_{2,Kepler}$	quadratic limb-darkening coeff	$0.240^{+0.075}_{-0.059}$		
Transit Parameters:		*Kepler*		
σ^2	Added Variance	$-0.000000000002^{+0.000000000037}_{-0.000000000036}$		
F_0	Baseline flux	$0.99999999^{+0.00000069}_{-0.00000070}$		

fraction of the code has been rewritten to be more flexible. EXOFASTv2 can now, among other things, simultaneously fit multiple planets, incorporate characterization observations (like Doppler Tomography), and simultaneously perform an SED within the global fit. EXOFASTv2 has a few major conceptual changes. First, the error scaling term for the transit photometry is now fit within the Markov chain Monte Carlo (MCMC). Also, the fit uses the stepping parameters $\log(M_*)$ and age instead of a/R_* and $\log g$. EXOFASTv2 has previously been used to determine parameters for the HD 106315 system (Rodriguez et al. 2017).

Because GJ 9827 is relatively low-mass with marginal applicability to both the Torres relations (Torres et al. 2010) and YY isochrones (Yi et al. 2001), we disable those constraints within the global model. To determine the mass and radius of GJ 9827, we interpolated the absolute K_S-band magnitude onto a grid of stellar evolutionary models and the semi-empirical M_K–M_* and M_K–R_* relations from Mann et al. (2015). We

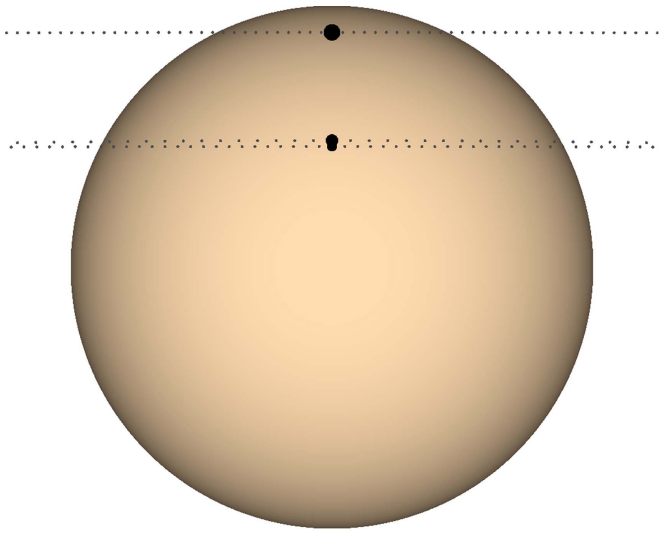

Figure 3. A diagram of the GJ 9827 system geometry shown with all planets at their respective transit centers. From top to bottom, the planets are d, b, and c. The color of the star matches its effective temperature, the planets are to scale with respect to each other and the host star, and the limb darkening matches our best-fit model in the *Kepler* band. The gray dots trace the orbital path of the planet, with a dot every three minutes. The curvature of planet b's orbit is plainly visible. Ω for each planet (a rotation of the path about the center of the star) is assumed to be zero. Note the mutual inclinations may be much larger than implied here due to the ambiguity between the inclination and 180° minus the inclination. Also note that, while this is the most likely model, the uncertainty in the impact parameters for planets b and c allow them to be non-overlapping (see Figure 4).

Table 3
The Best Confirmed Planets for Transmission Spectroscopy with $R_P < 3\ R_\oplus$

Planet	$R_P(R_\oplus)$	S/N[a]	References
GJ 1214 b	2.85 ± 0.20	1.00	Charbonneau et al. (2009)
55 Cnc e[b]	1.91 ± 0.08	0.41	Dawson & Fabrycky (2010)
HD 97658 b	$2.34^{+0.17}_{-0.15}$	0.36	Dragomir et al. (2013)
TRAPPIST-1f	1.045 ± 0.038	0.24	(Gillon et al. 2017)
GJ 9827b	$1.62 \pm 0.11\ R_\oplus$	0.14	this work
HD 3167 c	$2.85^{+0.24}_{-0.15}$	0.14	Vanderburg et al. (2016b), Christiansen et al. (2017)
HIP 41378 b	2.90 ± 0.44	0.14	Vanderburg et al. (2016a)
GJ 9827d	$2.07 \pm 0.14\ R_\oplus$	0.13	this work
K2-28 b	2.32 ± 0.24	0.12	Hirano et al. (2016)
HD 106315 b	2.5 ± 0.1	0.10	(Crossfield et al. 2017; Rodriguez et al. 2017)

Notes.
[a] The predicted signal-to-noise ratios relative to GJ 1214 b. All values used in determining the signal-to-noise were obtained from the NASA Exoplanet Archive (Akeson et al. 2013). If a system did not have a reported mass on NASA Exoplanet Archive or it was not a 2σ result, we used the Weiss & Marcy (2014) Mass–Radius relationship to estimate the planet's mass.
[b] Our calculation for the S/N of 55 Cnc e assumes an H/He envelope, as it falls just above the pure rock line determined by Zeng et al. (2016). However, 55 Cnc e is in an ultra short period orbit, making it unlikely that it would hold onto a thick H/He envelope.

assumed a main-sequence but unknown age (0.5–10 Gyr), a metallicity of -0.15 ± 0.2, and a solar [α/Fe]. This metallicity is based on the star's color–magnitude position (Neves et al. 2012) and *JHK* colors (Mann et al. 2013; Newton et al. 2014). However, the *K*-band is selected specifically because it shows a weak dependence with M_* and R_*, so adopting a lower metallicity as found by our spectral fitting does not significantly change the result. We tried both the Mesa Isochrones and Stellar Tracks (Choi et al. 2016; Dotter 2016) and Dartmouth Stellar Evolution Program (DSEP; Dotter et al. 2008) models, yielding radii of $0.60 \pm 0.02\ R_*$ and $0.59 \pm 0.03\ R_*$ and masses of $0.63 \pm 0.03\ M_*$ and $0.61 \pm 0.04\ M_*$, respectively. The relations from Mann et al. (2015), which are anchored in radii from long-baseline optical interferometry (Boyajian et al. 2012), produced a radius estimate of $0.64 \pm 0.03\ R_*$ and mass of $0.66 \pm 0.02\ M_*$. Errors account for uncertainties in the parallax and K_S-band magnitude.

GJ 9827 lands in a region of parameter space where weak molecular bands can form, where models are known to systematically underestimate the radii. However it also lands at the bright limit of the Mann et al. (2015) relations, around which the calibration stars are preferentially metal-rich when compared to GJ9827 (which would lead to an overestimated radius). Instead, we adopt more conservative parameters of 0.63 ± 0.03 M_* and 0.61 ± 0.03R R_* for GJ 9827, which encompass all values above with comparable uncertainties. These values for R_* and M_* were used as priors for the global fit.

We performed a separate global fit using the broad band photometry summarized in Table 1, the *Hipparcos* parallax, an upper limit on extinction from Schlegel et al. (1998), to derive the radius of the star. This fit recovered a consistent stellar radius and uncertainty to Houdebine et al. (2016), but the stellar metallicity was driven too high, perhaps biased unfairly by the lack of SED models for such metal-poor stars.

From the Houdebine et al. (2016) analysis of HARPS South spectra combined with an SED analysis of GJ 9827, we set a prior on $T_{\rm eff}$ of 4270 ± 100 K. Additionally, we imposed a prior on the parallax from *Hipparcos* (van Leeuwen 2007). Such a metal-poor, low-mass star may suffer from systematic biases in the limb darkening and gaps in the parameter tables. While a small error in the limb darkening is well within the uncertainty of the K2 light curve, allowing it to be fit within the global fit may work backward to bias the $\log g$, $T_{\rm eff}$, and [Fe/H] from which they are derived. Therefore, while the limb darkening values can be derived within EXOFASTv2 using the Claret & Bloemen (2011), we place a uniform prior of $\mu 1 = 0.44 \pm 0.1$ and $\mu 2 = 0.26 \pm 0.1$. The starting values were determined using the EXOFAST online tool[8] Eastman et al. (2016).

The system parameters determined from our global fit are shown in Table 2 and a diagram of the system geometry is shown in Figure 3.

4. Statistical Validation

To validate the planetary nature of the candidates identified to be transiting GJ 9827, we use the statistical techniques of Morton (2012) implemented in the `vespa` software package (Morton 2015). Using the location of the system in the sky and observational constraints, `vespa` calculates the astrophysical false positive probability (FPP) of the transiting planet candidates. This takes into account the possibility of hierarchical companions or background objects that could lead to a false identification of a transiting planet. Because GJ 9827 hosts multiple planets it is very unlikely that all three planet candidates are false positives.[9] Previous works have calculated

[8] http://astroutils.astronomy.ohio-state.edu/exofast/limbdark.shtml
[9] However, the chance that one of them is a false positive is harder to rule out (Latham et al. 2011).

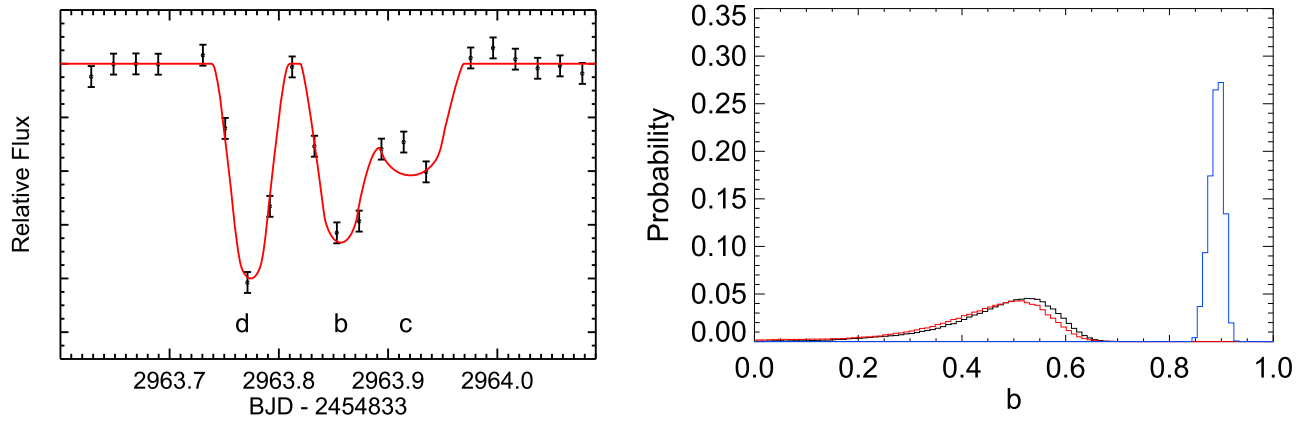

Figure 4. Left panel: the corrected K2 light curve for GJ 9827 showing a simultaneous transit of b and c with the EXOFASTv2 model shown in red. Right panel: the probability distribution of the impact parameter for GJ 9827 b (black), c (red), and d (blue). We cannot rule out the possibility of mutual transits of GJ 9827 b and c.

a "multiplicity boost" that reduces the FPP for multi-planet systems transiting a star in the original *Kepler* and *K2* fields (Lissauer et al. 2012; Sinukoff et al. 2016; Vanderburg et al. 2016b). After applying the multiplicity boost to the `vespa` determined FPP for the planets transiting GJ 9827, we estimate an FPP of 2×10^{-6}, 6×10^{-7}, and 6×10^{-10} for b, c, and d. Therefore, GJ 9827 b, c, and d are validated exoplanets.

5. Discussion

The proximity of GJ 9827 and its planetary architecture make it a compelling system worth further characterization. At ≈30 pc, this is the closest exoplanet system discovered by *K2* to date and one of the few stars to have multiple transiting terrestrial sized exoplanets that are well-suited for both mass measurements and atmospheric characterization. The host star is quite bright ($V = 10.3$, $J = 8$) and the measured planet radii of GJ 9827 b, c, and d are $1.62 \pm 0.11\,R_\oplus$, $1.269^{+0.087}_{-0.089}\,R_\oplus$, and $2.07 \pm 0.14\,R_\oplus$. As mentioned before, there is a known dichotomy in the sizes of short period (<100 days) small planets where planets are more commonly found to be less than $1.5\,R_\oplus$ or larger than $2.0\,R_\oplus$ (Fulton et al. 2017). Based on the mass measurements of planets in these two regimes, the larger planets are less dense and consistent with having an H/He envelope. It is thought that planets smaller than $\sim 1.6\,R_\oplus$ have lost this outer H/He envelope, leaving the rocky core, explaining their higher densities and a lack of planets with radii of 1.5–2.0 $R_\oplus$ (Weiss & Marcy 2014; Rogers 2015). The three known planets orbiting GJ 9827 provide a rare opportunity to perform a comparative study, as GJ 9827 c is $<1.5\,R_\oplus$, GJ 9827 d is $>2.0\,R_\oplus$, and GJ 9827 b lands right in this deficiency gap. This system may shed light on the evolution of planets within this radius regime.

Using the Weiss & Marcy (2014) mass–radius relations, we estimate the mass of GJ 9827 b, c, and d to be $4.26^{+0.54}_{-0.49}\,M_\oplus$, $2.63^{+1.59}_{-1.00}\,M_\oplus$, and $5.32^{+0.68}_{-0.62}\,M_\oplus$, respectively. Within our global model, EXOFASTv2 estimated the masses using the Chen & Kipping (2017) mass–radius relations to be $3.52^{+1.4}_{-0.93}\,M_\oplus$, $2.46^{+0.89}_{-0.75}\,M_\oplus$, and $5.2^{+2.1}_{-1.5}\,M_\oplus$. We note that the Weiss & Marcy (2014) planet mass uncertainties ignore any uncertainty in the mass–radius relation itself and are only due to the uncertainty in the radius. The Chen & Kipping (2017) estimated masses correspond to RV semi-amplitudes of $2.34^{+0.90}_{-0.54}\,\mathrm{m\,s^{-1}}$, $1.08^{+0.44}_{-0.25}\,\mathrm{m\,s^{-1}}$, and $2.01^{+0.79}_{-0.48}\,\mathrm{m\,s^{-1}}$. Houdebine et al. (2016) measured the rotational velocity of GJ 9827 to be $<2\,\mathrm{km\,s^{-1}}$, making the planets around GJ 9827 well-suited for precise RV observations with current spectroscopic facilities to measure their masses. The rotation period of GJ 9827 is either 31 days or 16 days, well separated from the orbital periods of the planets, so it should be possible to filter away signals from stellar activity using techniques like Gaussian process regression (Haywood et al. 2014).

To better understand the feasibility of characterizing the atmospheres of the three planets orbiting GJ 9827, we calculate the atmospheric scale height and an expected signal-to-noise per transit following the description given in Vanderburg et al. (2016b). We repeat this calculation for all known planets where $R_p < 3\,R_\oplus$ using NASA's Exoplanet archive (Akeson et al. 2013). It is expected that both GJ 9827 b and d might have thick gaseous atmospheres (Weiss & Marcy 2014), while GJ 9827 d likely does not have a thick envelope. We find that GJ 9827 b and d are two of the best small ($R_p < 3\,R_\oplus$) exoplanets for detailed atmospheric characterization (see Table 3).[10] By studying their atmospheric compositions, we may better understand the observed dichotomy in planetary composition observed at $\sim 1.6\,R_\oplus$. All calculations are done using the *H*-band magnitude of the stars to test the feasibility of characterizing the planet's atmosphere with the *Hubble Space Telescope's* Wide Field Camera 3 instrument and the upcoming suite of instruments that will be available on the *James Webb Space Telescope*. At a *J*-band magnitude of 8, GJ 9827 is near the expected saturation limit of the *JWST* instruments but should be accessible to all four instrument suites allowing for a high S/N with a relatively short exposure time: Near Infared Camera (NIRCam), Near Infrared Imager and Slitless Spectrograph (NIRISS), Near-Infrared Spectrograph (NIRSpec), and the Mid-Infrared Instrument (MIRI) (Beichman et al. 2014). The brightness of the GJ 9827 system makes it a great target for NIRCam's Dispersed Hartmann Sensor mode (Schlawin et al. 2017).

The short orbital periods of the three GJ 9827 planets and the near 1–3 period commensurability between GJ 9827 b and c provides opportunities to observe overlapping transits of the three planets, as shown in Figure 4. The simultaneous transit on UT 2017 February 11 of GJ 9827 b and c shows one discrepant

[10] We note that signal to noise is not everything. This calculation makes no assumptions about clouds or the presence of high-mean molecular weight atmospheres. The potential pitfalls of making these assumptions are illustrated by GJ 1214, which according to our calculation is the most amenable small planet to atmospheric characterization, but which shows no atmospheric features, likely due to the presence of clouds, hazes, or aerosols (Kreidberg et al. 2014).

data point that misses the EXOFASTv2 model. This kind of discrepancy might be explained by a mutual transit, where GJ 9827 c actually transits both GJ 9827 and planet b simultaneously, which is not modeled by EXOFASTv2. However, at the observed time of this observation, the transit of planet b likely would have already completed (unless there was a significant transit timing variation). We do not find any convincing evidence of mutual transits in our analysis but based on the probability of each planet's impact parameters (see Figure 4), we are not able to rule out this possibility.

6. Conclusion

We present the discovery of three transiting planets orbiting the nearby late K-type star, GJ 9827. Two of the three planets are in near resonance orbits with periods of 1.2 days and 3.6 days, while the outer planet has a period of 6.2 days. All three planets are super-Earth in size with radii of $1.62 \pm 0.11\,R_{\oplus}$, $1.269^{+0.087}_{-0.089}\,R_{\oplus}$, and $2.07 \pm 0.14\,R_{\oplus}$, for GJ 9827 b, c, and d, respectively. At only 30 pc from the Sun, this is the closest exoplanet system discovered by the *K2* mission. The proximity and brightness of the host star combined with the similarity in the size of the three transiting planets make GJ 9827 an excellent target for comparative atmospheric characterization. The expected radial velocity semi-amplitudes of the three planets are small but detectable with current instrumentation, especially given the star's fairly bright optical magnitude of $V = 10.25$. Radial velocity observations should be undertaken to measure the mass of each planet, to determine their interior structures for comparative studies. Mass measurements will also be critical for properly interpreting any atmospheric characterization through transit spectroscopy.

We thank Laura Kriedberg and Caroline Morley for their valuable conversations. Work performed by J.E.R. was supported by the Harvard Future Faculty Leaders Postdoctoral fellowship. This work was performed in part under contract with the California Institute of Technology (Caltech)/Jet Propulsion Laboratory (JPL) funded by NASA through the Sagan Fellowship Program executed by the NASA Exoplanet Science Institute. This paper includes data collected by the *Kepler*/K2 mission. Funding for the *Kepler* mission is provided by the NASA Science Mission directorate. Some of the data presented in this paper were obtained from the Mikulski Archive for Space Telescopes (MAST). STScI is operated by the Association of Universities for Research in Astronomy, Inc., under NASA contract NAS5–26555. Support for MAST for non-HST data is provided by the NASA Office of Space Science via grant NNX13AC07G and by other grants and contracts. Some of the data presented herein were obtained at the WM Keck Observatory (which is operated as a scientific partnership among Caltech, UC, and NASA). The authors wish to recognize and acknowledge the very significant cultural role and reverence that the summit of MaunaKea has always had within the indigenous Hawaiian community. We are most fortunate to have the opportunity to conduct observations from this mountain.

Note added in review. During the referee process of this paper, our team became aware of another paper reporting the discovery of a planetary system orbiting GJ 9827 (Niraula et al. 2017).

ORCID iDs

Joseph E. Rodriguez https://orcid.org/0000-0001-8812-0565
Andrew Vanderburg https://orcid.org/0000-0001-7246-5438
Jason D. Eastman https://orcid.org/0000-0003-3773-5142
Andrew W. Mann https://orcid.org/0000-0003-3654-1602
David W. Latham https://orcid.org/0000-0001-9911-7388
Samuel N. Quinn https://orcid.org/0000-0002-8964-8377

References

Akeson, R. L., Chen, X., Ciardi, D., et al. 2013, PASP, 125, 989
Batalha, N. M., Rowe, J. F., Bryson, S. T., et al. 2013, ApJS, 204, 24
Beichman, C., Benneke, B., Knutson, H., et al. 2014, PASP, 126, 1134
Benneke, B., Werner, M., Petigura, E., et al. 2017, ApJ, 834, 187
Boyajian, T. S., von Braun, K., van Belle, G., et al. 2012, ApJ, 757, 112
Brown, T. M. 2001, ApJ, 553, 1006
Burrows, A. S. 2014, Natur, 513, 345
Charbonneau, D., Berta, Z. K., Irwin, J., et al. 2009, Natur, 462, 891
Chen, J., & Kipping, D. 2017, ApJ, 834, 17
Choi, J., Dotter, A., Conroy, C., et al. 2016, ApJ, 823, 102
Christiansen, J. L., Clarke, B. D., Burke, C. J., et al. 2015, ApJ, 810, 95
Christiansen, J. L., Vanderburg, A., Burt, J., et al. 2017, AJ, 154, 122
Claret, A., & Bloemen, S. 2011, A&A, 529, A75
Crossfield, I. J. M., Ciardi, D. R., Isaacson, H., et al. 2017, arXiv:1701.03811
Crossfield, I. J. M., Ciardi, D. R., Petigura, E. A., et al. 2016, ApJS, 226, 7
Cutri, R. M., Skrutskie, M. F., van Dyk, S., et al. 2003, yCat, 2246, 0
Cutri, R. M., et al. 2014, yCat, 2328, 0
Dawson, R. I., & Fabrycky, D. C. 2010, ApJ, 722, 937
Dotter, A. 2016, ApJS, 222, 8
Dotter, A., Chaboyer, B., Jevremović, D., et al. 2008, ApJS, 178, 89
Dragomir, D., Matthews, J. M., Eastman, J. D., et al. 2013, ApJL, 772, L2
Dressing, C. D., & Charbonneau, D. 2015, ApJ, 807, 45
Eastman, J. 2017, EXOFASTv2: Generalized Publication-quality Exoplanet Modeling Code, Astrophysics Source Code Library, ascl:1710.003
Eastman, J., Gaudi, B. S., & Agol, E. 2013, PASP, 125, 83
Eastman, J. D., Beatty, T. G., Siverd, R. J., et al. 2016, AJ, 151, 45
Fortney, J. J., Sudarsky, D., Hubeny, I., et al. 2003, ApJ, 589, 615
Fulton, B. J., Petigura, E. A., Howard, A. W., et al. 2017, AJ, 154, 109
Gardner, J. P., Mather, J. C., Clampin, M., et al. 2006, SSRv, 123, 485
Gillon, M., Jehin, E., Lederer, S. M., et al. 2016, Natur, 533, 221
Gillon, M., Triaud, A. H. M. J., Demory, B.-O., et al. 2017, Natur, 542, 456
Hadden, S., & Lithwick, Y. 2014, ApJ, 787, 80
Hadden, S., & Lithwick, Y. 2017, AJ, 154, 5
Haywood, R. D., Collier Cameron, A., Queloz, D., et al. 2014, MNRAS, 443, 2517
Henden, A. A., Levine, S., Terrell, D., & Welch, D. L. 2015, in AAS Meeting 225 Abstracts, 336.16
Hirano, T., Fukui, A., Mann, A. W., et al. 2016, ApJ, 820, 41
Høg, E., Fabricius, C., Makarov, V. V., et al. 2000, A&A, 355, L27
Houdebine, E. R., Mullan, D. J., Paletou, F., & Gebran, M. 2016, ApJ, 822, 97
Howard, A. W., Marcy, G. W., Bryson, S. T., et al. 2012, ApJS, 201, 15
Howell, S. B., Sobeck, C., Haas, M., et al. 2014, PASP, 126, 398
Jin, S., & Mordasini, C. 2017, arXiv:1706.00251
Johnson, D. R. H., & Soderblom, D. R. 1987, AJ, 93, 864
Kreidberg, L., Bean, J. L., Désert, J.-M., et al. 2014, Natur, 505, 69
Latham, D. W., Rowe, J. F., Quinn, S. N., et al. 2011, ApJL, 732, L24
Lissauer, J. J., Marcy, G. W., Rowe, J. F., et al. 2012, ApJ, 750, 112
Mann, A. W., Brewer, J. M., Gaidos, E., Lépine, S., & Hilton, E. J. 2013, AJ, 145, 52
Mann, A. W., Feiden, G. A., Gaidos, E., Boyajian, T., & von Braun, K. 2015, ApJ, 804, 64
Marcy, G. W., Isaacson, H., Howard, A. W., et al. 2014, ApJS, 210, 20
Montet, B. T., Morton, T. D., Foreman-Mackey, D., et al. 2015, ApJ, 809, 25
Morton, T. D. 2012, ApJ, 761, 6

Morton, T. D. 2015, VESPA: False Positive Probabilities Calculator, Astrophysics Source Code Library, ascl:1503.011
Morton, T. D., & Swift, J. 2014, ApJ, 791, 10
Murray-Clay, R. A., Chiang, E. I., & Murray, N. 2009, ApJ, 693, 23
Neves, V., Bonfils, X., Santos, N. C., et al. 2012, A&A, 538, A25
Newton, E. R., Charbonneau, D., Irwin, J., et al. 2014, AJ, 147, 20
Niraula, P., Redfield, S., Dai, F., et al. 2017, AJ, 154, 266
Owen, J. E., & Jackson, A. P. 2012, MNRAS, 425, 2931
Owen, J. E., & Wu, Y. 2017, ApJ, 847, 29
Petigura, E. A., Howard, A. W., & Marcy, G. W. 2013, PNAS, 110, 19273
Reddy, B. E., Lambert, D. L., & Allende Prieto, C. 2006, MNRAS, 367, 1329
Reid, I. N., Hawley, S. L., & Gizis, J. E. 1995, AJ, 110, 1838
Rodriguez, J. E., Zhou, G., Vanderburg, A., et al. 2017, AJ, 153, 256
Rogers, L. A. 2015, ApJ, 801, 41
Schlawin, E., Rieke, M., Leisenring, J., et al. 2017, PASP, 129, 015001
Schlegel, D. J., Finkbeiner, D. P., & Davis, M. 1998, ApJ, 500, 525
Seager, S., & Sasselov, D. D. 2000, ApJ, 537, 916
Sinukoff, E., Howard, A. W., Petigura, E. A., et al. 2016, ApJ, 827, 78
Skrutskie, M. F., Cutri, R. M., Stiening, R., et al. 2006, AJ, 131, 1163
Sperauskas, J., Bartašiūtė, S., Boyle, R. P., et al. 2016, A&A, 596 A116
Thompson, S. E., Coughlin, J. L., Hoffman, K., et al. 2017, arXiv:1710.06758
Tian, F., Toon, O. B., Pavlov, A. A., & De Sterck, H. 2005, ApJ, 621 1049
Torres, G., Andersen, J., & Giménez, A. 2010, A&ARv, 18, 67
Vanderburg, A., Becker, J. C., Kristiansen, M. H., et al. 2016a, ApJL, 827, L10
Vanderburg, A., Bieryla, A., Duev, D. A., et al. 2016b, ApJL, 829, L9
Vanderburg, A., & Johnson, J. A. 2014, PASP, 126, 948
Vanderburg, A., Latham, D. W., Buchhave, L. A., et al. 2016c, ApJS, 222, 14
van Leeuwen, F. 2007, A&A, 474, 653
Weiss, L. M., & Marcy, G. W. 2014, ApJL, 783, L6
Wu, Y., & Lithwick, Y. 2013, ApJ, 772, 74
Yelle, R. V. 2004, Icar, 170, 167
Yi, S., Demarque, P., Kim, Y.-C., et al. 2001, ApJS, 136, 417
Zacharias, N., Monet, D. G., Levine, S. E., et al. 2004, BAAS, 36, 1418
Zeng, L., Sasselov, D. D., & Jacobsen, S. B. 2016, ApJ, 819, 127